Clusters of Transmembrane Residues Are Critical for Human Prostacyclin Receptor Activation†

Jeremiah Stitham, Aleksandar Stojanovic, Lauren A. Ross, Anthony C. Blount Jr., and John Hwa*

Departments of Pharmacology & Toxicology and of Medicine (Cardiology), Dartmouth Medical School, Hanover, New Hampshire 03755

Received February 12, 2004; Revised Manuscript Received May 11, 2004

ABSTRACT: Relaxation of vascular smooth muscle and prevention of blood coagulation are mediated by ligand-induced activation of the human prostacyclin (hIP) receptor, a seven-transmembrane-domain G-protein-coupled receptor (GPCR). In this study, we elucidate the molecular requirements for receptor activation within the region of the ligand-binding pocket, identifying transmembrane residues affecting potency. Eleven of 30 mutated residues in the region of the ligand-binding domain exhibited defective activation (decreased potency). These critical residues localized to four distinct clusters (analysis via a rhodopsin-based human prostacyclin receptor homology model). Residues $Y75^{2.65}$ (TMII), $F95^{3.28}$ (TMIII), and $R279^{7.40}$ (TMVII) comprised the immediate binding-pocket cluster and were shown to be essential for proper receptor activation, compared to equivalent expression levels of the wild-type hIP (WT $EC_{50} = 1.2 \pm 0.1$ nM; $Y75^{2.65}A$ $EC_{50} = 347.3 \pm 62.8$ nM, $p < 0.001$; $F95^{3.28}A$ $EC_{50} = 8.0 \pm 0.6$ nM, $p < 0.001$; $R279^{7.40}A$ $EC_{50} = 130 \pm 63.0$ nM, $p < 0.001$). Residues $S20^{1.39}$ (TMI), $F24^{1.43}$ (TMI), and $F72^{2.62}$ (TMII) were localized to a cluster involving $P17^{1.36}$, a critical residue thought to facilitate transmembrane movement during changes in activation conformation. A third cluster formed around amino acid $D60^{2.50}$ (TMII), containing the highly conserved (100% of prostanoid receptors) $D288^{7.49}/P289^{7.50}$ motif located in TMVII. Last, a large hydrophobic cluster composed of aromatic residues $F146^{4.52}$ (TMIV), $F150^{4.56}$ (TMIV), $F184^{5.40}$ (TMV), and $Y188^{5.44}$ (TMV) was observed away from the ligand-binding pocket, but still necessary for hIP activation. These results assist in delineating the potential molecular requirements for agonist-induced signaling through the transmembrane domain. Such observations may be generally applicable, as many of these clusters are highly conserved among the prostanoid receptors as well as other class A GPCRs.

Prostacyclin (PGI_2)[1] is a cyclooxygenase metabolite of arachidonic acid and plays many important roles within the cardiovascular system, including promotion of vascular smooth muscle relaxation and inhibition of platelet adhesion. In this capacity, PGI_2 works as a key antagonistic modulator to the vasoconstrictive and prothrombotic properties of thromboxane A_2 (TXA_2), the other major cyclooxygenase product and lipid mediator involved in maintaining vascular homeostasis (*1*). In humans, PGI_2 activity is mediated through a membrane-associated G-protein-coupled receptor (GPCR), known as the hIP, or human prostacyclin receptor. Upon binding its native ligand, the hIP undergoes conformational changes within its seven transmembrane domains, leading to activation of G-protein through the cytoplasmic domain. The G-protein most commonly associated with the hIP is Gs, which (upon activation) stimulates membrane-bound adenylyl cyclase (AC) to catalyze the formation of the second messenger cyclic AMP (cAMP) from intracellular stores of ATP. In turn, cAMP binds to and activates protein kinase A (PKA), whose catalytic domains are capable of downstream protein phosphorylation leading to vascular homeostasis (*2*). Recent *in vitro* studies have also demonstrated hIP coupling to Gq, stimulating the production of 1,2-diacylglycerol (DAG) and inositol 1,4,5-triphosphate (IP_3) via phospholipase C (PLC) (*3*). However, the physiological relevance of Gq-mediated hIP signaling remains unclear.

Using site-directed mutagenesis and molecular modeling, we have recently determined four residues within the upper half of the transmembrane domain that are required for proper agonist binding—$R279^{7.40}$ (TMVII), $F278^{7.39}$ (TMVII), $Y75^{2.65}$ (TMII), and $F95^{3.28}$ (TMIII) (*4*). These residues constitute the functional domain of the ligand-binding pocket for the hIP receptor and serve as key determinants of binding affinity. However, the role of these (and neighboring) residues in overall receptor activation, beyond their immediate ligand-binding contributions, has yet to be determined.

† This work was supported by a start-up grant provided by the Department of Pharmacology & Toxicology, Dartmouth Medical School (J.H.), American Heart Association Scientist Development Grant 0235260N (J.H.), American Heart Association Predoctoral Fellowship Grant 0315291T (J.S.), a PhRMA Foundation Predoctoral Fellowship Grant (A.S.), and a Dartmouth College Presidential Scholarship (L.A.R.).

* To whom correspondence should be addressed at the Department of Pharmacology & Toxicology. Phone: (603) 650-1813. Fax: (603) 650-1129. E-mail: John.Hwa@Dartmouth.edu.

[1] Abbreviations: GPCR, G-protein-coupled receptor; PGI_2, prostaglandin I_2 or prostacyclin; hIP, human prostacyclin receptor; TM, transmembrane; TXA_2, thromboxane A_2; AC, adenylyl cyclase; cAMP, cyclic adenosine monophosphate; PKA, protein kinase A; PLC, phospholipase C; DAG, 1,2-diacylglycerol; IP_3, inositol 1,4,5-triphosphate; DMEM, Dulbecco's modified Eagle's medium. The names of 20 amino acids are designated by their one-letter nomenclature.

10.1021/bi0496788 CCC: $27.50
Published on Web 06/26/2004

Helical movements, particularly those within TMIII and TMVI, have been shown to be necessary for proper activation of rhodopsin and β_2-adrenergic (β_2-AR) and parathyroid hormone receptors (*5*−*7*). More recent studies of both α_1-adrenergic (α_1-AR) and β_2-AR receptors have implicated particular phenylalanine residues (F303 and F282, respectively) as key facilitators in coupling TM helical movements to receptor and G-protein activation (*8*, *9*). Moreover, such phenylalanine (and tryptophan) residues located within the binding pockets of the α_1-AR and serotonin (5-HT_2) receptors have also been shown to play an important role in receptor activation by stabilizing aromatic portions of their respective ligands (*10*, *11*). In our own investigations of the hIP receptor, we have demonstrated that transmembrane prolines also play a critical role in facilitating such helical movements, serving as molecular hinge points, which allow inter- and intra-α-helical movements. Moreover, such evidence suggests that helical movements arising from ligand binding initiate the activation cascade (*12*). With receptor activation necessitating a conformational change, we propose that activation-modulating residues within the vicinity of the ligand-binding pocket initiate the activation process (upon ligand binding), providing a point of origin, while more outlying amino acids serve to propagate the signal either as direct members of the signal-transfer chain or as indirect, structural stabilizers. This analysis, in association with a previously developed molecular homology model, provides critical insights into the transmembrane requirements for hIP receptor activation.

Our findings support the assertion that a number of ligand-dependent activation clusters are required for proper receptor activation. These clusters are located in various sections of the transmembrane domain—both in close proximity to and distant from the immediate ligand-binding pocket. These clusters can be highly conserved (across GPCRs), with closely associated critical conserved proline or phenylalanine residues, or can be unique to the human prostacyclin receptor. This study supports the hypothesis that there are common components for receptor activation across GPCRs, in addition to those found exclusively in the prostacyclin receptor.

EXPERIMENTAL PROCEDURES

Materials. Iloprost ligands—radiolabeled [^{3}H]iloprost (17.0 Ci/mmol) and nonradiolabeled iloprost—were purchased from Amersham Biosciences (Piscataway, NJ). Oligonucleotide primers were purchased from Sigma-Genosys (The Woodlands, TX), while the hIP cDNA was a generous gift from Dr. Mark Abramovitz (Merck Frosst, Quebec, Canada).

Construction of Mutant Receptors. Human IP cDNA was cloned into the plasmid vector pMT4, and point mutations were generated using conventional methods of PCR mutagenesis (*13*). Complementary oligonucleotide primers were designed extending 10−12 nucleotides 3′ and 5′ from the desired mutation site. The PCR reaction mixture contained 1× Pfu reaction buffer, 200 ng of DNA construct, 150 ng of each primer (sense and antisense), 10 mM dNTPs, and 2.5 units of Pfu DNA polymerase (Stratagene, Austin, TX), and was heated and cooled at 95 °C for 30 s, 55 °C for 1 min, and 68 °C for 10 min for 16 cycles. The products were then digested with *Dpn*I restriction enzyme (Promega, Madison, WI) for 3 h to remove any parental wild-type strands of DNA. A 10 μL sample of PCR product was used to transform competent DH5α *E. coli* cells (∼2 × 10^9 cells), followed by DNA extraction from selected clones. Large plasmid preparations were performed using Wizard Plus Maxiprep kits (Promega), and all mutant constructs were confirmed via PCR DNA dideoxynucleotide chain-termination sequencing (Molecular Biology Core Facility, Dartmouth Medical School, Hanover, NH).

Transfection of COS-1 Cells. Transient transfections were performed on COS-1 cells as follows: The initial wash of cells with Cellgro Dulbecco's modified Eagle's medium (DMEM; Mediatech, Inc., Herndon, VA) was followed by addition of mutant DNA in diethylaminoethyl-Dextran (DEAE-Dextran; Sigma, St. Louis, MO) (0.2 mg/mL DMEM). Cells were then incubated at 37 °C with 5% CO_2 for 6 h, after which 0.1 mM chloroquine solution was added. Cells were subsequently incubated for 1 h, and chloroquine was removed through washes with DMEM. Cells were harvested 72 h post-transfection.

Membrane Preparations. Preparations of COS-1 cell membranes were carried out as previously described (*12*). In brief, cells were washed in phosphate-buffered saline (PBS) and harvested using cell scrapers. Vortexing (providing shear forces) for 3 min in sucrose (0.25 M) was followed by a low-speed spin (∼1260*g*) for 5 min, and the supernatant was collected. After a high-speed centrifugation (∼30000*g* for 15 min) the pellet was then washed twice in 1× HEM (20 mM HEPES, pH 7.4, 1.5 mM EGTA, and 12.5 mM $MgCl_2$), followed by resuspension in 1× HEM containing 10% glycerol, and stored at −70 °C. A Bradford protein assay was performed to quantitate membrane proteins.

Ligand Binding. Ligand-binding characteristics for the COS-1-expressed and human-platelet-derived receptors were determined through a series of competition binding assays using the radiolabeled ligand [^{3}H]iloprost. Analysis involved construction of reaction mixtures (in duplicate wells) containing 50 μg of COS-1 membrane or 30 μL of human blood (10000 platelets), HEM buffer, and 15 nM [^{3}H]iloprost, along with 1 of 11 different concentrations of cold (nonradiolabeled) iloprost, ranging from 10 μM to 0.1 nM. After 1.5 h of incubation at 4 °C, reactions were stopped by the addition of ice-cold 10 mM Tris/HCl buffer (pH 7.4) and filtered onto Whatman GF/C glass-fiber filters, using a Brandel cell harvester. The filters were washed five times with ice-cold Tris/HCl buffer, and radioactivity was measured in the presence of 5 mL of Ecoscint H scintillation fluid (National Diagnostics, Atlanta, GA). Nonspecific binding was determined by the addition of a 200-fold excess of nonradiolabeled iloprost. Saturation binding studies were performed using [^{3}H]iloprost concentrations between 1 and 100 nM. Data were analyzed using GraphPad Prism software (GraphPad Software, Inc., San Diego, CA). IC_{50} values were converted to K_i using the Cheng−Prusoff equation, and K_i values were expressed as a mean ± SE. Analysis of variance (ANOVA with post-test Newman−Keuls) and Student's *t* tests were used to determine significant differences ($p < 0.05$). It should be noted that the membrane preparations also contain a proportion of intracellular membranes. Thus, detected receptor numbers may not completely reflect those on the cell surface.

cAMP Determination. The wild-type hIP with the epitope tag (hIP1D4) and mutant constructs were analyzed for signal transduction capabilities. COS-1 cells were transiently trans-

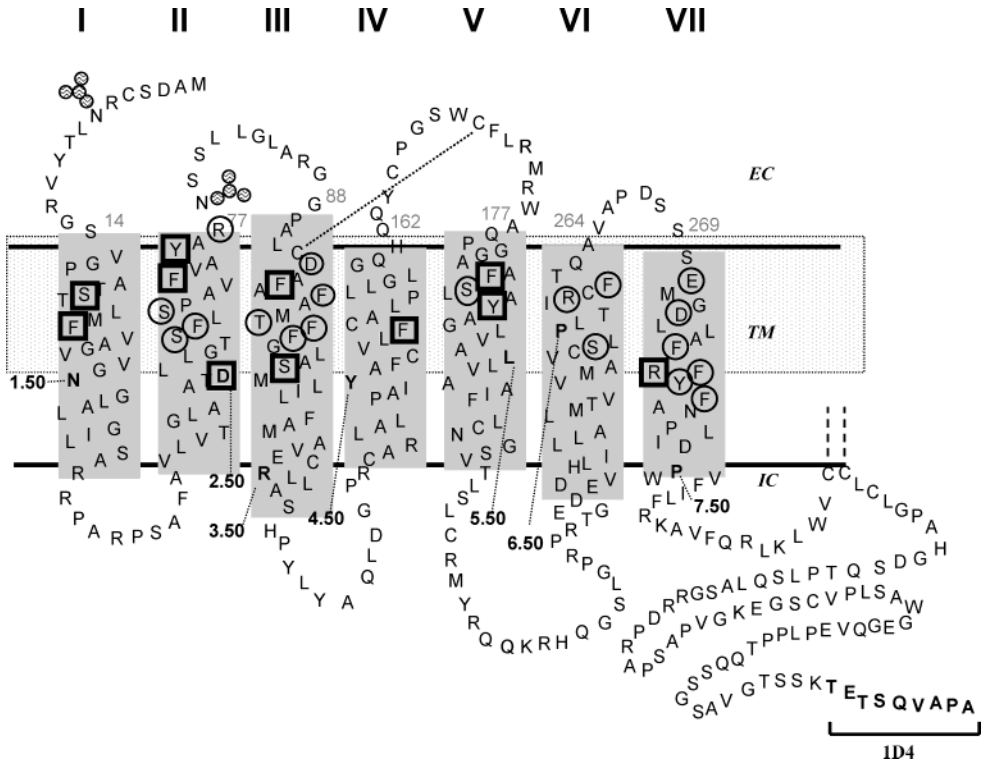

FIGURE 1: Mutation sites on the secondary structure of the hIP receptor. Diagram highlighting the positions for 30 putative binding-pocket residues within the upper half of the seven transmembrane helical domains (shaded boxes). Extracellular, transmembrane, and cytoplasmic regions are designated on the basis of the X-ray crystallographic structure of rhodopsin, with approximate membrane boundaries numbered. The conserved disulfide bond, found in the extracellular domain, is indicated with a dashed line, as are the two palmitoylation sites, located along the cytoplasmic domain. The small circles indicate the two glycosylation sites. The C-terminus has been tagged with a 1D4 epitope (bold). A shaded box highlights the region for the putative ligand-binding pocket. Shown in bold squares are the residues that showed a significant difference in iloprost activation when mutated to alanine, as compared to the wild-type hIP1D4 protein. Shown in circles are the residues that are unaffected by such an alanine mutation. Bold letters represent the most conserved residues within each respective transmembrane α-helix, $N31^{1.50}$, $D60^{2.50}$, $R117^{3.50}$, $Y186^{4.50}$, $L194^{5.50}$, $P274^{6.50}$, and $P289^{7.50}$.

fected with 2 μg of receptor DNA in 25 mm plates as described above. After 72 h, the cells were washed twice with PBS plus 4 mM EDTA and 2 mM IBMX (Sigma) (pH 7.4) and incubated at 20 °C for 10 min. This was followed by addition of defined concentrations of iloprost to selected plates. For the assays on platelets (in whole blood), each reaction contained 90 μL of whole blood, one-sixth (15 μL) of which was used in the final cAMP determination. This 15 μL is equivalent to approximately 5000 platelets. Dose−response curves were determined by the addition of six different iloprost concentrations (1 μM to 10 pM) in duplicate. After 20 min the cells were harvested and boiled for 3 min followed by high-speed (10000 rpm) centrifugation. A 50 μL sample of the resultant supernatant (total of 300 μL) was used to determine cAMP production in the competition assay. Cyclic AMP levels were measured using the radioreceptor competition assay (Amersham). In brief, [^{3}H]cAMP was used in competition for a cAMP-binding protein against known concentrations of nonradiolabeled cAMP, followed by determination of the unknowns. The reaction was allowed to proceed for 2 h at 4 °C. Charcoal was used to remove excess unbound cAMP. Samples were counted in 5 mL of Ecoscint H (National Diagnostics). Results were analyzed with GraphPad Prism software. For the dose−response assay, a nonlinear, curve-fitting program (GraphPad Prism) was used and the EC_{50} (mean ± SE) determined for wild-type hIP1D4 and mutant constructs. Analysis of variance and Student's *t* tests were used to determine statistically significant differences ($p < 0.05$).

Immunofluorescence Microscopy. COS-1 cells were seeded into six-well tissue culture plates containing sterilized glass cover slips, and transiently transfected with varying concentrations of wild-type hIP1D4 (1.0, 0.5, 0.25, and 0.025 μg/mL) and mutant $Y75^{2.65}A$ (2.0 and 1.0 μg/mL) DNA, according to the aforementioned transfection protocol. Cells were fixed and permeabilized 48 h post-transfection in 100% methanol (5 min), followed by ice-cold acetone at −20 °C for 5 min. Receptors were labeled using 1D4 monoclonal antibody (1:1000 dilution, for 60−90 min), followed by goat antimouse IgG AlexaFluor488 fluorescent antibody (Molecular Probes, Inc., Eugene, OR) (1:1000 dilution, for 60−90 min). Cells were examined via confocal microscopy directly following preparation, using a Bio-Rad (Hercules, CA) MRC-1024 krypton/argon laser confocal system. Fluorescent cells were counted within each high-powered field (40×) containing approximately 100 cells. The mean ± SE was obtained for each transfection level. Results were compared and analyzed using a Student's *t* test.

Analysis of the hIP Receptor Homology Model and Model-Based Predictions. A computer-generated, three-dimensional homology model of the seven transmembrane α-helices of the hIP receptor, based upon the 2.8 Å resolution X-ray crystal structure of rhodopsin (PDB code 1HZX), was constructed using the Internet-based protein-modeling server SWISS-MODEL (GlaxoSmithKline, Geneva, Switzerland) (*4*, *14*, *15*). Visualization and evaluation of our hIP model was performed using the Swiss PDB Viewer (GlaxoSmithKline). Mutations that affect activation were analyzed for

potential interactions with neighboring amino acids. Of particular interest were those residues in the region of the putative binding pocket known to directly interact with the prostacyclin ligand. Such analysis allowed for further predictions and additional mutagenesis within the proximal region.

Amino Acid Numbering Scheme. The generalized numbering scheme used throughout the manuscript is based upon the common GPCR indexing system (*16*), whereby the relative position of each amino acid is designated by a sequence-identifying number. Such numbers begin with the transmembrane α-helix number (1−7) followed by a relative position number, which is based upon a reference residue that comprises the most conserved amino acid within a particular transmembrane α-helix (across all class A rhodopsin-like GPCRs). By definition, the most conserved residue is assigned the number "50". Thus, other amino acid positions relative to these conserved reference numbers are assigned increasing values (above 50) as they proceed toward the C-terminal tail of the receptor, while those residues that recede in the direction of the N-terminus decrease in value (below 50). In the case of the human prostacyclin receptor, an asparagine residue at position 31 within the first transmembrane α-helix (TMI) is the most conserved residue, and is thus designated N31$^{1.50}$. The respective conserved amino acids for the other transmembrane domains are D60$^{2.50}$, R117$^{3.50}$, Y186$^{4.50}$, L194$^{5.50}$, P274$^{6.50}$, and P289$^{7.50}$ (Figure 1).

Association and Dissociation Experiments. Association and dissociation experiments were performed to assess for potential differences in binding kinetics between wild-type hIP and mutant F278$^{7.39}$A. For association experiments, membranes expressing 1 pmol of hIP/mg of membrane protein were incubated with 1 mL of 1× HEM buffer and 40 nM [^{3}H]iloprost on ice. At time intervals of 1, 5, 30, and 60 min, 100 μL fractions (in duplicate) were spun (10000 rpm for 1 min), and the membrane pellet was washed quickly with 1 mL of ice-cold 10 mM Tris, pH 7.4. The pellet was then resuspended in 100 μL of 10 mM Tris/HCl and radioactivity counted using 5 mL of Ecoscint H liquid scintillation fluid. For dissociation experiments, membranes expressing 1 pmol of hIP/mg of membrane protein were incubated at 0 °C for 1.5 h with 1 mL of 1× HEM buffer and 40 nM [^{3}H]iloprost. The cells were then centrifuged at 10000 rpm to pellet the membranes, and the supernatant was replaced with 1 mL of fresh ice-cold 1× HEM without iloprost. At time points 1, 5, 10, 30, and 60 min, 100 μL aliquots (in duplicate) were centrifuged at 10000 rpm, and the radioactivity of the pellet was counted with 5 mL of Ecoscint H liquid scintillation fluid. The dissociation half-life was estimated from a single-exponential dissociation curve fit (GraphPad Prism). Experiments were performed at 0 °C to slow the rapid ligand off-rates, and a 1 min centrifugation was employed to pellet the membrane protein for scintillation counting. Relatively low concentrations of [^{3}H]iloprost (40 nM) were used to prevent high background counts. Significant differences ($p < 0.05$) were determined by statistical analysis using a Student's *t* test.

RESULTS

Our goal in this study was to assess the transmembrane requirements for hIP activation. Taking into account our previous work, in which 29 transmembrane-resident amino acids were evaluated for effects on agonist-binding affinity (*4*), this study focuses upon effects on potency (EC_{50}), by way of cAMP production, to determine those residues central to hIP receptor signal transduction activation (Table 1).

Table 1: Binding, Expression, and Activation of the Human Prostacyclin Receptor and Its Mutants[a]

amino acid identifier	mutation residue change	potency $EC_{50} \pm$ SEM (nM) (*n*)	affinity[b] $K_i \pm$ SEM (nM) (*n*)	B_{max}[b] (pmol/mg)	prostacyclin interactions
	wild type	1.2 ± 0.1 (10)	7.9 ± 1.7 (9)	1.8	
2.65	Y75A	347 ± 62 (4)[e]	>500 (6)[e]	0.5	C11-OH
3.28	F95A	8.0 ± 0.6 (3)[e]	143 ± 98 (6)[c]	0.8	ω-chain
7.39	F278A	2.5 ± 0.7 (7)	295 ± 80 (6)[d]	0.8	rings
7.39	F278W	2.2 ± 0.5 (6)	9.4 ± 1.2 (4)	0.5	rings
7.40	R279A	130 ± 63 (3)[e]	>500 (5)[e]	0.5	C1-COOH
1.36	P17A	6.3 ± 1.3 (3)[c]	12.8 ± 4.4 (5)	1.7	
1.39	S20A	32.8 ± 4.9 (4)[e]	8.7 ± 2.3 (3)	1.6	
1.43	F24A	19.0 ± 2.7 (4)[e]	4.9 ± 1.3 (3)	1.2	
1.50	N31A	32 ± 12.6 (4)[e]	314 ± 68 (3)[c]	0.6	
2.50	D60A	32.8 ± 8.1 (4)[e]	>500 (5)[e]	0.1	
2.55	S65A	1.9 ± 0.7 (3)	5.1 ± 1.7 (3)	2.2	
2.56	F66A	4.6 ± 1.1 (5)	12.4 ± 3.4 (4)	1.0	
2.58	S68A	3.7 ± 0.7 (3)	62.3 ± 28.5 (4)[d]	1.2	
2.62	F72A	5.2 ± 0.8 (5)[d]	7.0 ± 2.7 (3)	0.4	
2.67	R77A	1.6 ± 0.4 (3)	4.0 ± 1.0 (3)	0.5	
3.26	D93A	1.7 ± 0.1 (3)	4.7 ± 2.0 (3)	1.8	
3.30	F97A	1.2 ± 0.5 (5)	80.3 ± 13.9 (3)[e]	0.6	
3.33	T100A	1.2 ± 0.1 (4)	4.0 ± 1.1 (3)	0.8	
3.34	F101A	1.2 ± 0.1 (4)	9.5 ± 1.9 (4)	0.4	
3.35	F102A	4.3 ± 1.2 (4)	4.2 ± 1.1 (3)	0.2	
3.39	S106A	5.3 ± 0.6 (6)[d]	7.1 ± 2.3 (4)	1.3	
4.52	F146A	5.3 ± 1.3 (3)[d]	25.0 ± 15.0 (3)	0.3	
4.56	F150A	23.7 ± 7.0 (3)[d]	>500 (4)[e]	0.1	
5.40	F184A	10.0 ± 2.9 (3)[d]	13.2 ± 5.6 (3)	0.2	
5.41	S185A	2.1 ± 0.1 (3)	85.8 ± 22.5 (5)[c]	0.2	
5.44	Y188A	12.0 ± 1.5 (5)[e]	>500 (5)[e]	0.2	
5.44	Y188L	NR (3)	>500 (3)[e]	0.3	
5.44	Y188S	NR (3)	19.9 ± 1.2 (3)	0.2	
5.44	Y188F	0.5 ± 0.2 (3)	9.1 ± 6.5 (3)	0.3	
6.48	S252A	0.8 ± 0.1 (3)	15.6 ± 6.0 (3)	0.6	
6.54	R258A	2.9 ± 0.6 (4)	8.3 ± 3.0 (3)	0.4	
6.56	F260A	3.5 ± 0.5 (3)	11.4 ± 4.7 (4)	1.4	
7.32	E271A	2.7 ± 0.5 (5)	18.7 ± 10.0 (3)	0.8	
7.35	D274A	2.8 ± 0.7 (5)	>500 (4)[e]	0.3	
7.41	F280A	1.1 ± 0.1 (3)	10.8 ± 4.3 (5)	0.9	
7.42	Y281A	0.8 ± 0.1 (3)	15.7 ± 8.1 (3)	2.1	
7.44	F283A	1.6 ± 0.3 (3)	6.2 ± 1.8 (4)	0.7	
7.49	D288A	8.5 ± 3.5 (3)[c]	74.3 ± 15.0 (3)[c]	0.6	

[a] Positions of mutations (TM location) correspond to Figure 1. Mutations other than those directly involved in ligand binding are arranged by amino acid sequence position. Shown are $EC_{50} \pm$ SEM and $K_i \pm$ SEM from at least three separate experiments (*n*). B_{max} was determined from the mean of at least two separate transfections using 2 μg of DNA/mL. ANOVA and Student's *t* tests were performed to determine the significance from the wild type. Indicated also are the critical residues that directly interact with the native ligand prostacyclin. NR = no cAMP response (Figure 5B). [b] Adapted from ref *4*. [c] $p < 0.05$. [d] $p < 0.01$. [e] $p < 0.001$.

Due to the large number of hIP mutants being analyzed, binding and dose−response assays were performed using a transiently transfected COS-1 cell system. Such methods have been used extensively for the structural and functional assessments of many other GPCRs (*17*−*20*); nevertheless, it was essential for us to validate the system for use with the hIP receptor. Potential activation-affecting residues were selected on the basis of position (vicinity of the ligand-binding pocket) as well as hydrophobic, polar, or charged side-chain characteristics (Figure 1). Eleven of the initial 30

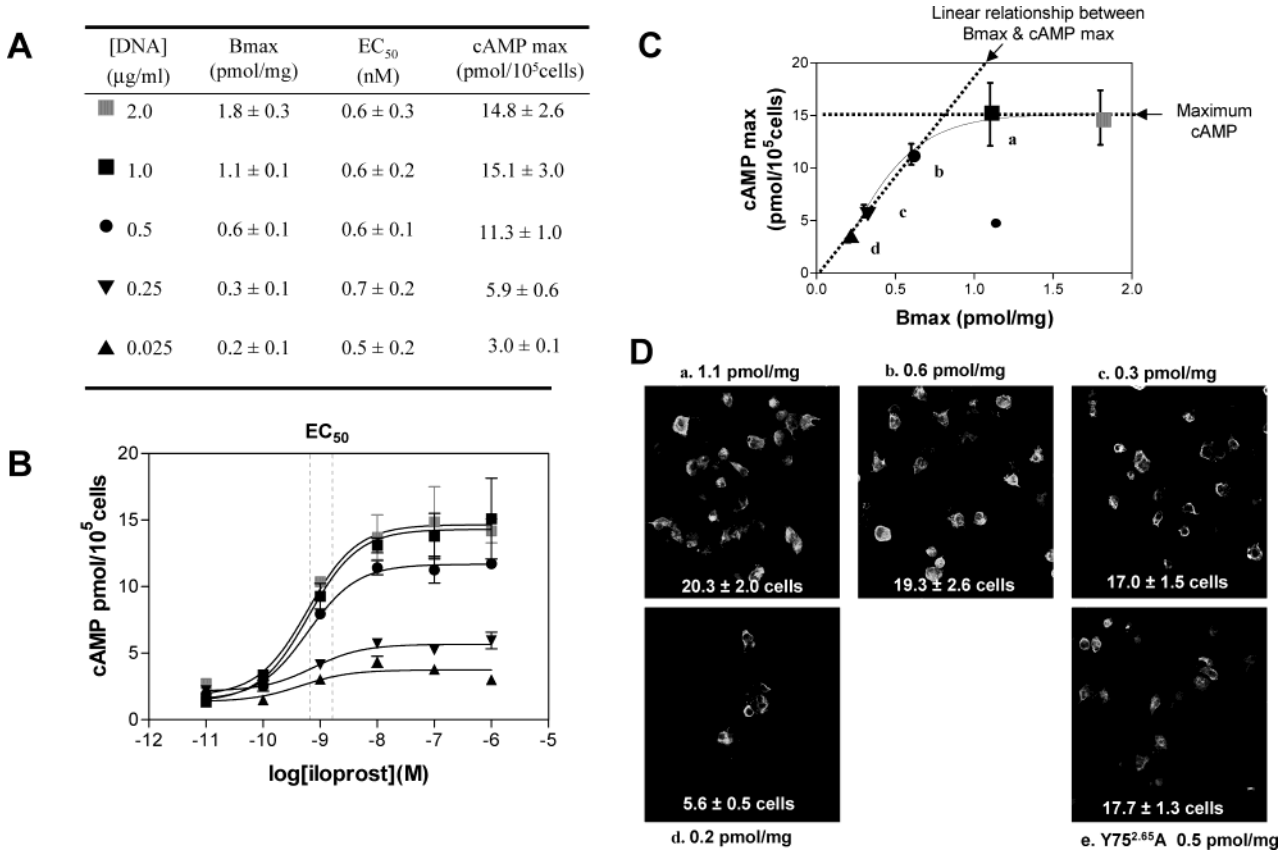

FIGURE 2: Wild-type hIP transfected into COS-1 cells at different DNA concentrations does not significantly affect EC_{50}. Panel A: Table describing DNA titration (2−0.025 μg/mL) in the COS-1 eukaryotic expression system via transient transfection. Corresponding receptor numbers were calculated (B_{max}) in addition to potency EC_{50} and cAMP maximum (maximal values attained at plateau) response values. Panel B: Curves corresponding to the expression levels outlined in panel A. Indicated by a dashed line is the calculated EC_{50} from nonlinear regression analysis for each individual transfection. EC_{50} values (concentration at which 50% activation is achieved) did not fluctuate in correspondence with varying maximal (100%) activation levels or receptor numbers (B_{max}). Panel C: Nonlinear regression plot of maximal cAMP attained at each expression level. Symbols used correspond to those from panels A and B. At low expression levels there is a linear relationship between cAMP maximum and expression hIP levels. At higher expression levels there is a maximal response observed (plateau). Letters (a−d) were designated for individual points (DNA concentration used in transfections). These letters also correspond to the confocal microscopy slides shown in panel D. Panel D: Confocal microscopy of COS-1 cells expressing fluorescent-labeled wild-type hIP1D4 (panels a−d) and $Y75^{2.65}A$ (panel e). Corresponding expression levels are shown above or below each respective panel. The number of fluorescent cells per high-powered field, mean ± standard error of the mean, is indicated in white within the panel. Shown are typical results obtained from at least three experiments.

residues examined exhibited a significant defect in Gs-coupled activation (i.e., decreased potency) when mutated to alanine, as determined via iloprost-induced cAMP generation (Table 1). Using a rhodopsin-based homology model of the hIP transmembrane domain, activation-critical residues were mapped three-dimensionally, *in silico* to identify potential patterns and/or mechanisms leading to signal transduction and receptor activation. Further mutagenesis and functional assays were employed to evaluate our observations. The results of these studies have begun to clarify the molecular components involved in coupling the processes of ligand binding to receptor activation and signal transduction.

Wild-Type hIP Expression Levels Can Arise from Both Increased Numbers of Transfected Cells and Increased Intracellular Receptor Expression; However, EC_{50} Is Not Significantly Affected at These Expression Levels (Figure 2). The dose−response assessment is complex and influenced by the agonist (ability to bind and activate—affinity and efficacy), the receptor (basal activity and capacity for agonist-induced activation—efficacy), and the cellular context (different dose responses when expressed in different cell lines) (*21*). Moreover, extraneous experimental conditions, such as aberrant drug accessibility or receptor numbers, can further complicate matters. By systematically using the same agonist within the same receptor-tissue expression system, we were able to achieve similar receptor expression levels (in the absence of significant spare receptors), leading to similar efficacy. Further validation of our approach was attained through a direct comparison between our eukaryotic COS-1 system and that of natively expressed hIP on human platelets.

Wild-type hIP receptor was transfected, in parallel, with five different concentrations of DNA (ranging from 0.025 to 2.0 μg/mL), leading to a progressive increase in hIP expression (B_{max}) from 0.2 to 1.8 pmol/mg of membrane protein (Figure 2A). Binding affinity (K_i, nM), as determined from competition binding studies, revealed no significant difference between the varying transfection levels and K_i values (7.9 ± 1.2 nM for 1.8 pmol/mg of membrane protein) (data not shown). Dose−response values (EC_{50}, nM) were obtained concurrently and also showed no significant difference among the various transfection levels (Figure 2A). Shown in Figure 2B are the dose−response curves for the corresponding hIP expression levels. Maximal cAMP production plateaued at the higher hIP expression levels (1.1

and 1.8 pmol), revealing nearly identical dose−response curves (Figure 2B) and cAMP maximum values. At lower expression levels, a linear relationship between cAMP maximum and expression levels (B_{max}) was observed (Figure 2C).

To explore whether receptor expression levels were due to an increase in the number of cells transfected, or simply an increase in the membrane protein being expressed per cell, confocal microscopy was performed using a monoclonal antibody against the 1D4 epitope tag (C-terminus of hIP). At lower expression levels, as observed with data points "d" to "c" (0.2−0.3 pmol/mg), there was a significant increase in the number of cells transfected (confocal microscopy) (Figure 2D). For expression levels of 0.2 pmol/mg, approximately 5.6 ± 0.5 (mean ± standard error of the mean (SEM), $n = 5$) cells per high-powered field (40×, containing approximately 100 total cells) exhibited fluorescence. At 0.3 pmol/mg expression, 17.0 ± 1.5 cells ($n = 3$) were observed, while 0.6 pmol/mg corresponded to 19.3 ± 2.6 cells ($n = 4$) and 1.1 pmol/mg corresponded to 20.3 ± 2.0 cells per high-powered field per high-powered field. At higher expression levels (data points "b" to "a" corresponding to 0.6−1.1 pmol/mg), there were no significant increases in the number of transfected cells, suggesting increased receptor expression per cell. This pattern of expression also correlated with the cAMP data, which have a linear relationship with rising expression levels, up to approximately 0.8 pmol/mg of membrane protein. However, this relationship seems to plateau at higher expression levels, where the number of receptors per cell dramatically increases. Moreover, it should be noted that, at these high expression levels, AC has been shown to be the rate-limiting component in cAMP production (*22*, *23*), as opposed to receptors or G-proteins. With expression patterns established for the wild-type hIP, we subsequently studied one of our mutant receptors to determine whether a similar trend in receptor expression occurred. The mutant chosen for examination was$Y75^{2.65}A$, a critical residue affecting ligand binding (interacts with prostacyclin C11-OH), receptor activation, and protein expression levels (Table 1). As seen in Figure 2D, panel e, $Y75^{2.65}A$ had a B_{max} value of 0.5 pmol/mg of membrane protein and showed cell number expression (17.7 ± 1.3 cells transfected per 40× field, $n = 3$) similar to that of the wild type in Figure 2D, panel c (wild-type $B_{max} = 0.3 \pm 0.1$ pmol/mg of membrane protein). Such analogous results, with both wild-type and mutant hIP, demonstrate that equivalent levels of expression (i.e., both the number of cells transfected and the number of receptors per cell) are achievable within our transient transfection system, although this was not assessed for every mutation. It should also be noted that B_{max} values were derived from surface-membrane-bound receptors in addition to a portion from intracellular compartment membranes, while EC_{50} values were derived from only surface-bound receptors. Thus, low maximal activity observed with some mutants may be, in part, due to intracellular retention. Nonetheless, our studies suggest that the EC_{50} values are comparable across wild-type and mutant receptors at the levels of expression under study.

EC_{50} and K_i Values for the COS-1 Cell Transfection System Reflect That Found on Human Platelets (Figure 3). In an attempt to verify whether results observed in our COS-1 cell overexpression system accurately reflected hIP in its native environment (i.e., on human platelets), a direct comparison of assay results from COS-1-cell- and human-platelet-derived hIP was performed. As can be seen in Figure 3, superimposition of the competition binding and dose−response nonlinear regression curves reveal the similarities between binding (IC_{50}) and activation (EC_{50}) for both receptor expression systems. The overall EC_{50} value for wild-type, COS-1-cell-expressed hIP was 1.2 ± 0.1 nM (mean ± SEM, $n = 10$) (Table 1, Figure 3A), which did not significantly differ from the EC_{50} values determined from human platelets (3.6 ± 0.9 nM, $n = 3$) (Figure 3B). In a like manner, no significant difference was observed in the binding affinity (K_i) for both systems: $K_i = 7.9 \pm 1.7$ nM ($n = 9$) for COS-1-expressed hIP and $K_i = 13.4 \pm 3.8$ nM, ($n = 3$) for human platelets. This correspondence in relationship further supports our COS-1 cell overexpression system as a valid model, suitably reflecting the physiological coupling of binding to activation, as seen in human-platelet-derived hIP. Thus, hIP receptors with single mutations were characterized for activation potency, in comparison to wild-type hIP, at equivalent levels of expression in the linear range (Figure 2C).

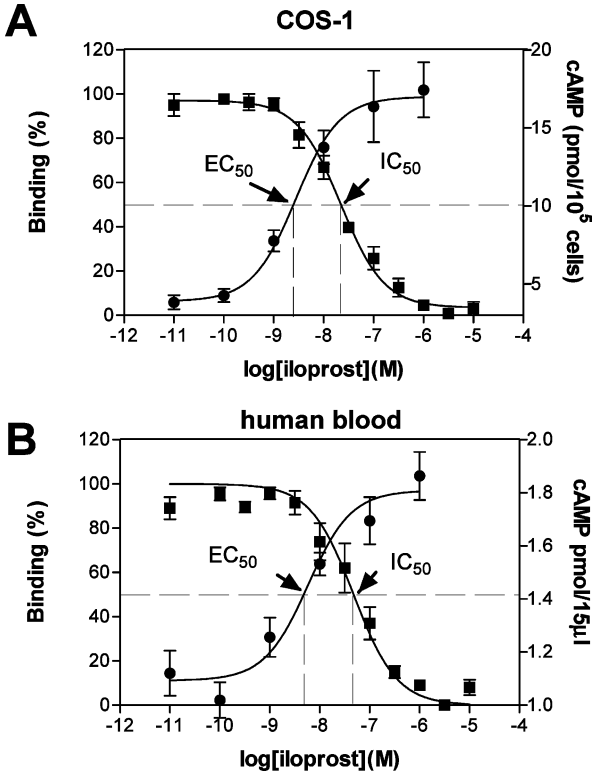

FIGURE 3: The COS-1 cell transfection system reflects native hIP found on human platelets. Competition binding curves for wild-type hIP (squares and left axis) were determined as outlined in the Experimental Procedures. The IC_{50} was established on the basis of best-fit single-slope nonlinear regression (GraphPad Prism) and 50% binding. Activation curves were also performed on the basis of production of cAMP (circles and right axis). The EC_{50} (50% activation) was determined using best-fit single-slope nonlinear regression (GraphPad Prism). Concentration differences between IC_{50} and EC_{50} are shown with dashed lines. Panel A highlights a transiently transfected hIP system in COS-1 cells. Shown is a typical experiment that has been reproduced 10 times. Panel B is for an experiment identical to that of panel A; however, human blood platelets (containing native hIP receptors) were used as an alternative. A 15 μL sample of blood contains approximately 5000 platelets.

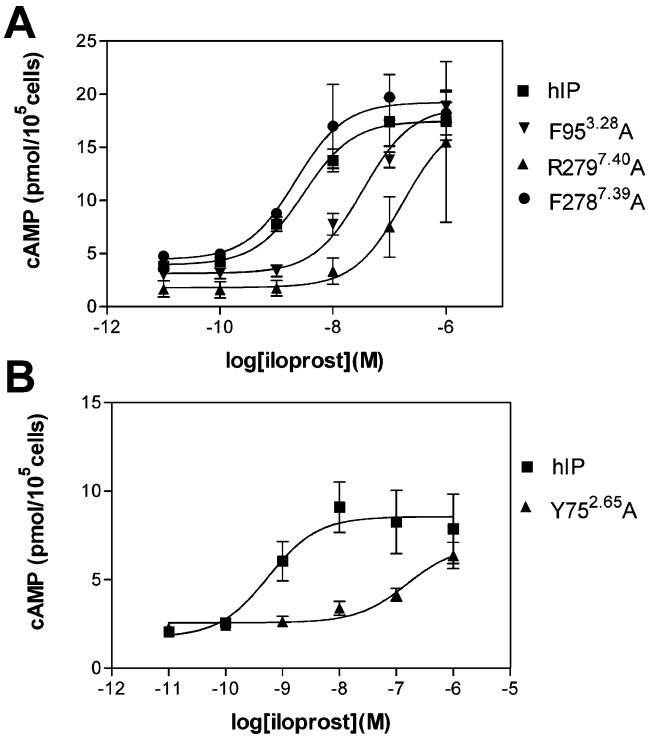

FIGURE 4: Effects of immediate binding-pocket residue mutations on hIP receptor activation. cAMP activation of immediate binding-pocket residue mutations F95$^{3.28}$A, F278$^{7.39}$A, and R279$^{7.40}$A (panel A) and Y75$^{2.65}$A (panel B**)**. Iloprost concentrations ranging from 1 μM to 0.01 nM were used. Results are the mean and standard error (pmol of cAMP/10^5 cells transfected) from one experiment, with constructs performed in parallel. EC_{50} was determined from the best-fit single-slope nonlinear regression curve (GraphPad Prism), and the results are shown in Table 1. At least three repetitions were performed, all showing similar results.

Binding-Pocket Cluster: Three of the Four Direct Ligand-Binding Amino Acids, Y75$^{2.65}$ (TMII), F95$^{3.28}$ (TMIII), and R279$^{7.40}$ (TMVII), Significantly Affect Receptor Activation (Figure 4). Upon mapping potency-affecting residues onto our rhodopsin-based, three-dimensional model of the hIP, a distinct cluster around the prostacyclin-binding domain was observed, involving three of the four previously identified immediate binding-pocket residues (Y75$^{2.65}$, F95$^{3.28}$, F278$^{7.39}$, and R279$^{7.40}$). Each exhibited a significant defect in activation upon mutation to alanine, as measured by cAMP generation, F95$^{3.28}$A (EC_{50} = 8.0 ± 0.6 nM, $p < 0.001$), Y75$^{2.65}$A (EC_{50} = 347.3 ± 62.8 nM, $p < 0.001$), and R279$^{7.40}$A (EC_{50} = 130 ± 63.0 nM, $p < 0.001$) (Table 1, Figure 4). Previous work has shown that these residues comprise the functional core of the ligand-binding pocket of the hIP and directly interact with ligand side-chain components: Y75$^{2.65}$ interacts with the C11-hydroxyl group of prostacyclin, F95$^{3.28}$ with the ω-chain, and R279$^{7.40}$ with the C1-carboxylate group (*4*). Further detailed analysis at the Y75$^{2.65}$ position, through secondary mutations to Y75$^{2.65}$F and Y75$^{2.65}$S (to assess the significance of the hydroxyl group versus the phenyl ring), showed further activation deficiencies (decreased potency, increased EC_{50}) with both secondary mutations (Y75$^{2.65}$F EC_{50} ± SEM = 77.5 ± 26.0 nM, n = 4, $p < 0.001$; Y75$^{2.65}$S EC_{50} ± SEM = 197.5 ± 51.9 nM, n = 4, $p < 0.001$), indicating the importance of both side-chain subconstituents—that is, the phenyl ring (size and hydrophobicity) and hydroxyl group (H-bonding capability)—to achieve full activation. Two other binding-pocket-resident amino acids assessed for effects on hIP activation were F97$^{3.30}$ (TMIII), which lends to the hydrophobic stabilization of the PGI_2 ω-chain, and D274$^{7.35}$ (TMVII), whose backbone carbonyl (C═O) appears to interact with the backbone amine hydrogen of F278$^{7.39}$. Despite significant contributions toward binding affinity for both residues, neither exhibited an observable impact on activation potency upon alanine mutation (F97$^{3.30}$A EC_{50} ± SEM = 1.2 ± 0.5 nM, n = 5; D274$^{7.35}$A EC_{50} ± SEM = 2.8 ± 0.7 nM, n = 5) (Table 1).

P17$^{1.36}$ Proximal Cluster: Residues S20$^{1.39}$ (TMI) and F72$^{2.62}$ (TMII) in Close Proximity to the Binding Pocket Are Necessary for Receptor Activation (Figures 6A and 8). The importance of the binding pocket is further highlighted by the activation defects associated with four neighboring amino acids located within TMI (P17$^{1.36}$, S20$^{1.39}$, F24$^{1.43}$) and TMII (F72$^{2.62}$) (Figure 6A and Table 1). Residue F72$^{2.62}$ is located one α-helical turn from the critical Y75$^{2.65}$ binding-pocket residue described above. When mutated to alanine (F72$^{2.62}$A), a consistent and significant activation defect was observed (EC_{50} ± SEM = 5.2 ± 0.8 nM, n = 5, $p < 0.01$). Interestingly, within our rhodopsin-based homology model, F72$^{2.62}$ is also positioned in close proximity to an important transmembrane proline residue, P17$^{1.36}$, shown in a previous study to be required for proper receptor activation (P17$^{1.36}$A EC_{50} ± SEM = 6.3 ± 1.3 nM, n = 3, $p < 0.05$) (*9*). Similarly, S20$^{1.39}$, whose hydroxyl side chain and/or carbonyl backbone appear to link it (via H-bonds) to P17$^{1.36}$ in our model, showed a significant decrease in receptor potency upon mutation (S20$^{1.39}$A EC_{50} ± SEM = 32.8 ± 4.9 nM, n = 4, $p < 0.001$). Residue F24$^{1.43}$, which is located one α-helical turn from amino acid S20$^{1.39}$, is the farthest outlier from the ligand-binding pocket (Figure 6A), but still maintains a significant effect on receptor activation (F24$^{1.43}$A EC_{50} ± SEM = 19.0 ± 2.7 nM, n = 4, $p < 0.001$). Amino acid S68$^{2.58}$, one α-helical turn below F72$^{2.62}$, demonstrated no decrease in potency upon mutation to alanine, but did show a significant adverse effect on binding affinity.

P289$^{7.50}$-Associated D60$^{2.50}$ Cluster: Residues N31$^{1.50}$ (TMI), D60$^{2.50}$ (TMII), and D288$^{7.49}$ (TMVII) in the Transmembrane Domain Are Necessary for Receptor Activation (Figures 6B and 8). Residue D60$^{2.50}$ (TMII) showed a significant effect on receptor activation when mutated to alanine (EC_{50} = 32.8 ± 8.1 nM, n = 4, $p < 0.001$). D60$^{2.50}$ comprises one member of a polar, three-residue cluster, along with amino acids D288$^{7.49}$ (TMVII) and N31$^{1.50}$ (TMI), whose side chains all appear to point inward toward each other, most likely offsetting charges in the formation of an inter-α-helical hydrogen-bonding network, or perhaps the sequestration of an internal water molecule (Figure 6B). Activation analysis of D288$^{7.49}$A in TMVII and N31A$^{1.50}$ shows EC_{50} values of 8.5 ± 3.5 nM (n = 3) ($p < 0.01$) and 32.0 ± 12.6 nM (n = 3) ($p < 0.001$), respectively. This residue is adjacent to P289$^{7.50}$, which also has a marked effect on receptor activation (P289$^{7.50}$A EC_{50} = 6.3 ± 2.2 nM, n = 3, $p < 0.05$) (*12*). The disruption of this polar cluster (via D60$^{2.50}$A mutation) may adversely affect the nearby proline P289$^{7.50}$ via D288$^{7.49}$, perhaps inhibiting its capacity to convey activation signals through a conformational change (α-helical movement), although further mechanistic analysis is required to confirm such an effect. D60$^{2.50}$, N31$^{1.50}$, D288$^{7.49}$, and P289$^{7.50}$ are all 100% conserved across the prostaglandin receptors.

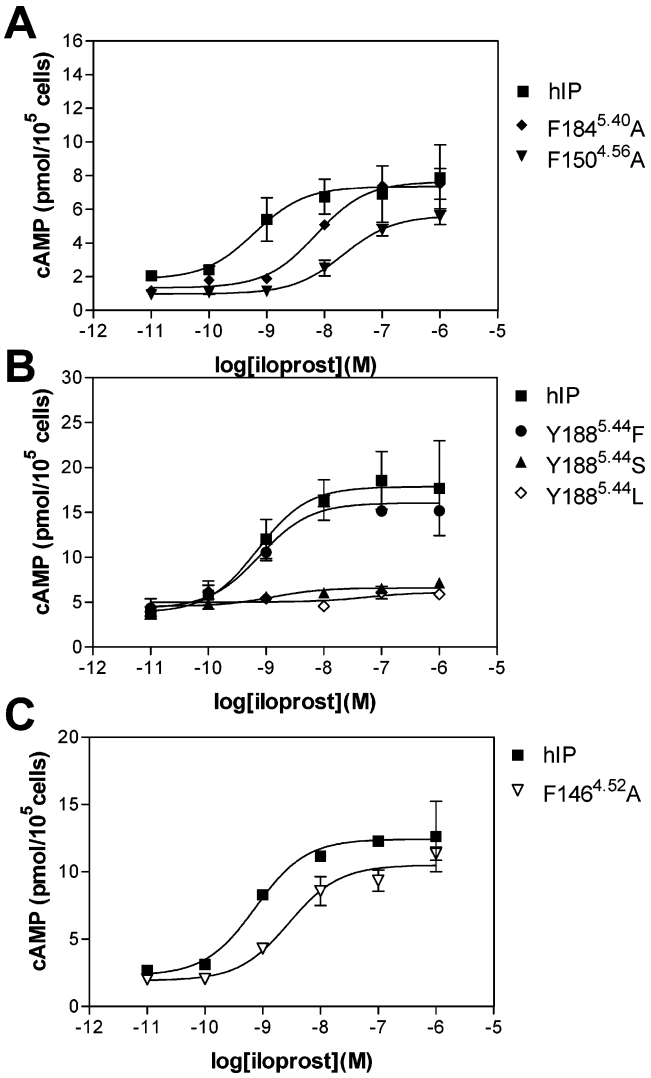

FIGURE 5: Effects of mutations in close proximity to the binding pocket on hIP receptor activation. cAMP activation assays were performed with mutations F150$^{4.56}$A and F184$^{5.40}$A (panel A), Y188$^{5.44}$F, Y188$^{5.44}$S, and Y188$^{5.44}$L (panel B), and F146$^{4.52}$A (panel C). Iloprost concentrations ranging from 1 μM to 0.01 nM were used. Results are the mean and standard error (pmol of cAMP/10^5 cells transfected) from one experiment, with constructs performed in parallel. EC_{50} was determined from best-fit single-slope nonlinear regression (GraphPad Prism). At least three repetitions were performed, all showing similar results.

Aromatic Cluster: Intra- and Inter-α-Helical Hydrophobic Ring−Ring Interactions between TMIV and TMV Are Critical for Receptor Activation (Figures 5, 6C, and 8). Three residues, F150$^{4.56}$, F184$^{5.40}$, and Y188$^{5.44}$, form a large hydrophobic cluster located away from the aforementioned immediate and proximal ligand-binding domains. When mutated to alanine, all had significant effects on activation, F150$^{4.56}$A (TMIV) ($EC_{50} = 23.7 \pm 7.0$ nM, $n = 3$, $p < 0.01$), F184$^{5.40}$A (TMV) ($EC_{50} = 10.0 \pm 2.9$ nM, $n = 3$, $p < 0.01$), and Y188$^{5.44}$A (TMV) ($EC_{50} = 12.0 \pm 1.5$ nM, $n = 5$, $p < 0.001$) (Table 1, Figure 5A,B). Analysis of our hIP structural model confirmed the location of this hydrophobic group between transmembrane domains TMIV and TMV (Figure 6C), and highlighted the potential involvement of F146$^{4.52}$, another large hydrophobic residue located on TMIV. Secondary mutations were performed for Y188$^{5.44}$ (to assess the significance of the hydroxyl group versus the phenyl ring),

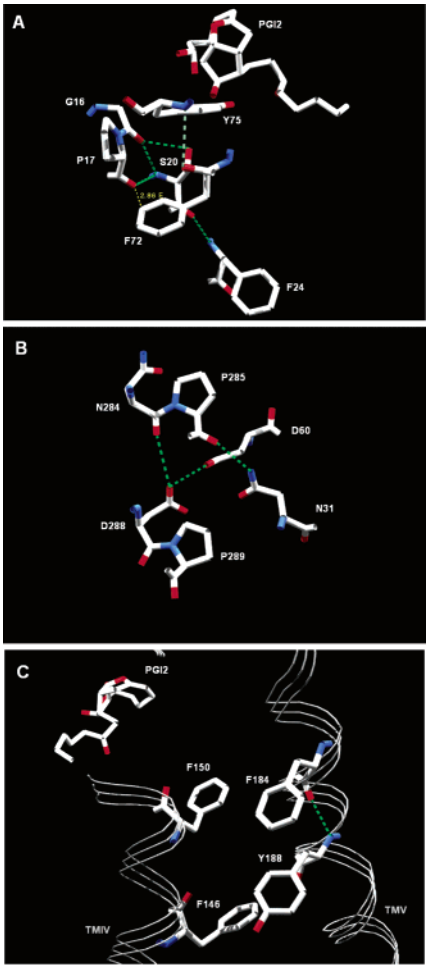

FIGURE 6: Computer-generated homology model of critical clusters required for hIP activation. Panel A: Y75$^{2.65}$-tethered, P17$^{1.36}$-associated hinge near the binding pocket. Computer-generated homology model of the hIP transmembrane domain region with significant effects on receptor activation. All other amino acids and α-helices have been removed for clarity. Shown is residue S20$^{1.39}$ (TMI), whose functional hydroxyl (−OH) group, as well as backbone amine, has the potential to hydrogen bond (green dashed lines) to the backbone carbonyl (C═O) oxygen of G16 (TMI), which lies directly adjacent to P17$^{1.36}$ (TMI). Also shown are residues F72$^{2.62}$and Y75$^{2.65}$ (both found in TMII). The intra-α-helical hydrogen bond connecting the F72$^{2.62}$ carbonyl (C═O) oxygen with the important Y75$^{2.65}$ binding-pocket residue (at the amine group) is depicted by gray dashed lines. Panel B: Polar amino acid cluster in close proximity to residues P285$^{7.46}$ and P289$^{7.50}$ (TMVII). Computer-generated homology model of the hIP transmembrane domain region with significant effects on receptor activation. All other amino acids and α-helices have been removed for clarity. Shown is a polar cluster comprised of three main residues with inward-oriented side chains, D60$^{2.50}$ (TMII), D288$^{7.49}$ (TMVII), and N31$^{1.50}$ (TMI). Green dashed lines highlight hydrogen bonding, between D60$^{2.50}$ and D288$^{7.49}$ functional side chains, as well as the N284$^{7.45}$ backbone carbonyl (C═O). Proline residues P285$^{7.46}$ and P289$^{7.50}$ (both TMVII) are also shown, with interactions between the N31$^{1.50}$ side-chain amine (NH_2) and P285$^{7.46}$ backbone carbonyl (C═O). Panel C: Hydrophobic stabilization of TMIV and TMV via aromatic residues. Computer-generated homology model of the hIP transmembrane domain region with significant effects on receptor activation. All other amino acids and α-helices have been removed for clarity. Shown are aromatic residues F146$^{4.52}$ and F150$^{4.56}$ (TMIV), along with F184$^{5.40}$ and Y188$^{5.44}$ (TMV). The adjacent stacks of aromatic residues support potential hydrophobic (ring−ring) interactions between amino acids F150$^{4.56}$ and F184$^{5.40}$, as well as F146$^{4.52}$ and Y188$^{5.44}$. The green dashed line represents an intra-α-helical hydrogen bond between the backbone components of amino acids F184$^{5.40}$ and Y188$^{5.44}$.

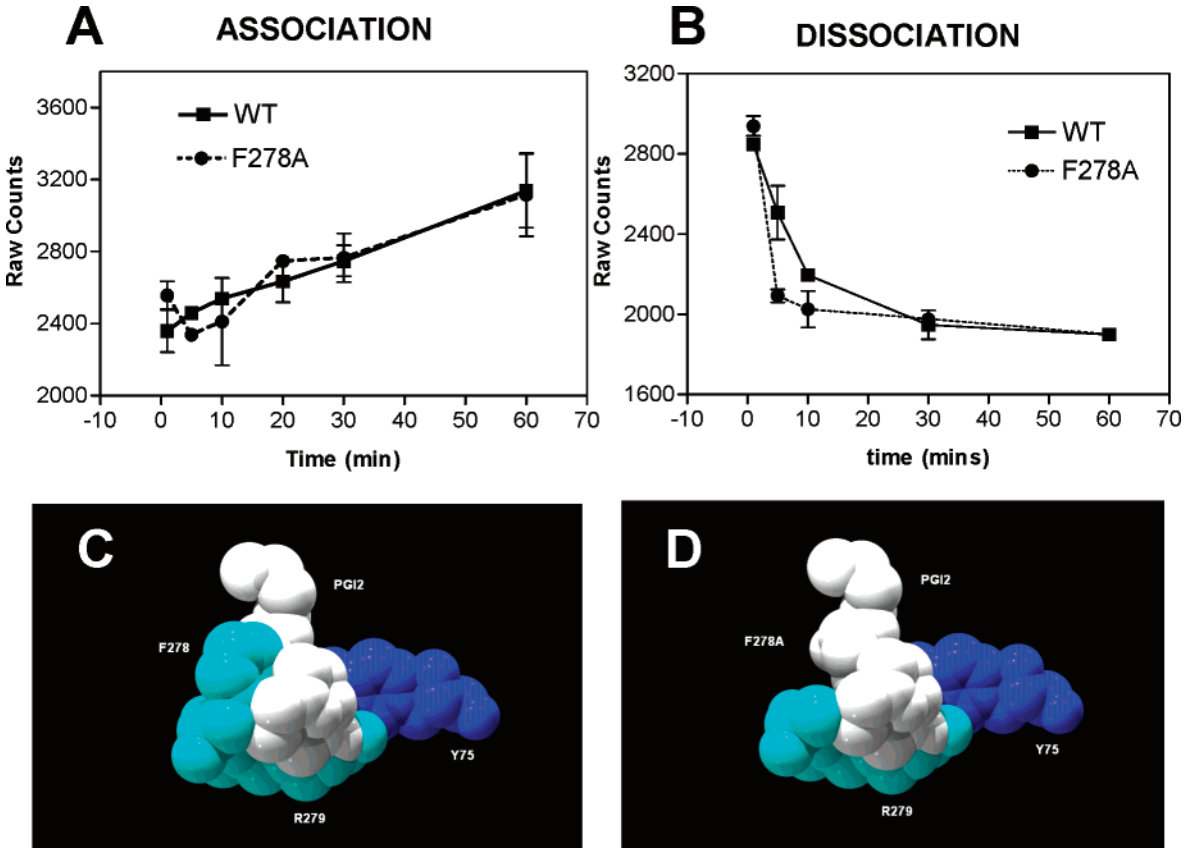

FIGURE 7: Association and dissociation experiments for the F278$^{7.39}$A mutation. Panel A: Association experiment for F278$^{7.39}$A and wild-type hIP using [^{3}H]iloprost. Changes in radioactivity counts (association) were measured over 60 min. Results shown are for one of three identical experiments, all showing no significant differences between F278$^{7.39}$A and wild-type hIP. Panel B: Dissociation of iloprost from F278$^{7.39}$A and wild-type hIP over a 60 min period. Similar results indicating significant differences between F278$^{7.39}$A and wild-type hIP were observed in three separate experiments. Panel C: Space-filling model showing the F278$^{7.39}$ acting as a "clamp" (central rings and α-tail) for prostacyclin. Panel D: Space-filling model showing that mutagenesis to F278$^{7.39}$A removes the clamp, allowing more rapid dissociation.

with the Y188$^{5.44}$F mutation exhibiting wild-type-like activation properties (EC_{50} = 0.5 ± 0.1 nM, n = 3). In contrast, significant activation deficiencies were observed with both the Y188$^{5.44}$S (n = 3) and Y188$^{5.44}$L (n = 3) mutations (Figure 5B), lending strong evidence for the requirement of a large hydrophobic residue at position 188. Upon mutation to alanine, F146$^{4.52}$A demonstrated a significant decrease in activation potency (EC_{50} = 5.3 ± 0.7 nM, n = 3, p < 0.01) (Figure 5C). As indicated by our model (Figure 6C), it appears that F146$^{4.52}$ is involved in a hydrophobic (ring−ring) interaction with Y188$^{5.44}$, which, in turn, seems to be interacting in a similar manner with F184$^{5.40}$, positioned approximately one α-helical turn above (toward the extracellular surface) on TMV. Additionally, F150$^{4.56}$ also appears to contribute to this large aromatic contingent (F146$^{4.52}$ and Y188$^{5.44}$), interacting with F184$^{5.40}$ (TMV). Taken together, the four aromatic residues F150$^{4.56}$, F184$^{5.40}$, Y188$^{5.44}$, and F146$^{4.52}$, which are highly conserved throughout all the prostanoid receptors, appear to be arranged in an interlocking planar stack, providing conformational stability for transmembrane α-helices TMIV and TMV through a hydrophobic effect.

Moreover, this interaction (stabilization) seems to be required for proper receptor activation. Residue S185$^{5.41}$, which is situated directly next to F184$^{5.40}$ in TMV, had no effect on receptor potency when mutated to alanine (EC_{50} = 2.1 ± 0.1 nM, n = 3).

Last, the only residue affecting receptor activation that we were unable to localize to a specific cluster was S106$^{3.39}$, located in TMIII (S106$^{3.39}$A EC_{50} = 5.3 ± 0.6, n = 6, p < 0.01) (Table 1). S106$^{3.39}$ is oriented away from all of the important clusters described with no apparent structural importance. However, TMIII itself does contain both the conserved ERY sequence (ERC in the hIP) and one of the cysteine residues (C92$^{3.25}$) involved in the putative disulfide bond between TMIII and TMV (C170$^{5.26}$ on the second extracellular loop) (Figure 1). Further detailed analysis of the region is required to establish its role in hIP activation.

F278$^{7.39}$A Leads to a More Rapid Agonist Dissociation Accounting for Decreased Affinity with Normal Potency (Figure 7). Contrary to expectations, mutation of the fourth and final binding-pocket residue (F278$^{7.39}$A) had little effect on receptor activation (EC_{50} ± SEM = 2.5 ± 0.7 nM, n = 7), despite eliciting a severe reduction in ligand-binding affinity (Figure 4A and Table 1). Such results, suggesting normal receptor activation in the absence of proper ligand binding, were both intriguing and perplexing. Moreover, there was no evidence of increased basal activity or constitutive activity with this mutation. One possible explanation for such a phenomenon might be that the decreased iloprost affinity observed with the F278$^{7.39}$A mutant may have arisen from an increased agonist off-rate, which was insufficient to affect the occupancy time required for activation. For potency (EC_{50}) to remain unchanged, both the minimum agonist-

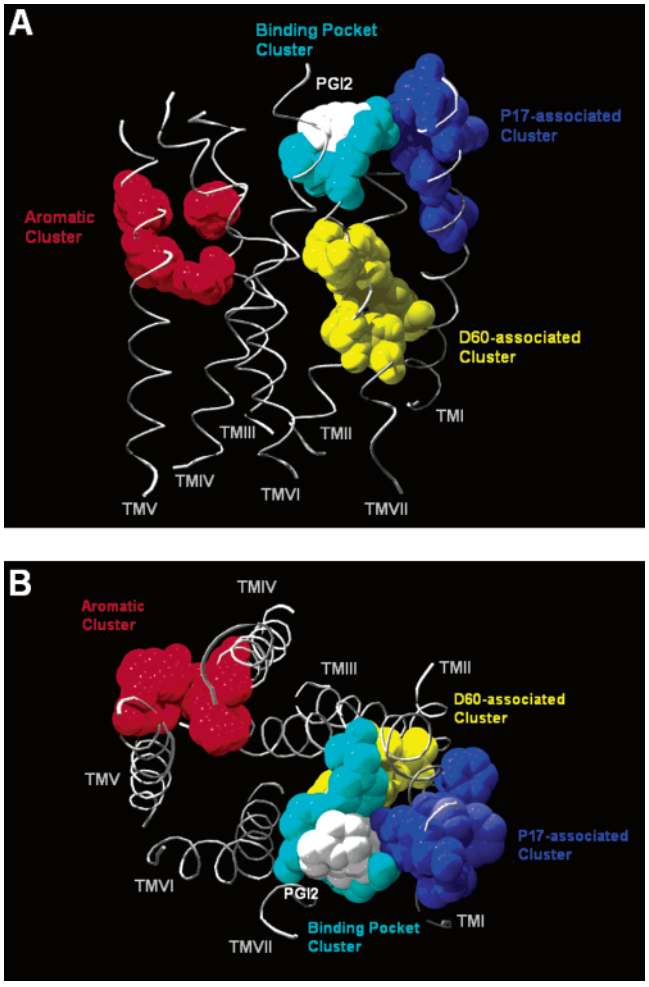

FIGURE 8: Computer-generated homology model of the hIP transmembrane domain with activation-affecting clusters. Panel A: Side view of transmembrane α-helices (gray corkscrews labeled TMI through TMVII) of the hIP receptor with bound PGI_2 ligand (white). Space-filled molecules represent the positions of activation-affecting residue clusters: binding-pocket cluster (light blue, $Y75^{2.65}$, $F95^{3.28}$, $F278^{7.39}$, and $R279^{7.40}$), $P17^{1.36}$-associated cluster (dark blue, $P17^{1.36}$, $S20^{1.39}$, $F24^{1.43}$, and $F72^{2.62}$), $D60^{2.50}$-associated cluster (yellow, $N31^{1.50}$, $D60^{2.50}$, $D288^{7.49}$, and $P289^{7.50}$), and aromatic cluster (red, $F146^{4.52}$, $F150^{4.56}$, $F184^{5.40}$, and $Y188^{5.44}$). Panel B: Overhead view (extracellular) of transmembrane α-helices (gray corkscrews labeled TMI through TMVII) of the hIP receptor with bound PGI_2 ligand (white). Space-filled molecules represent the positions of the same activation-affecting residue clusters shown in panel A.

binding time required for receptor activation and the number of receptors occupied would have to remain the same for both the $F278^{7.39}$A mutant and wild-type hIP. As a result, association and dissociation experiments were performed to determine whether there were any changes in ligand-binding kinetics that may support this hypothesis. The results from duplicate time points in three separate experiments revealed no significant differences in the rate of agonist association for either the wild-type or mutant $F278^{7.39}$A receptor (Figure 7A). However, clear differences in dissociation rates (Figure 7B) were observed between the two receptors, with the $F278^{7.39}$A mutant dissociating its ligand nearly 8 times faster (dissociation $t_{1/2} = 0.7 \pm 0.25$ min, $n = 3$) than the wild-type hIP (dissociation $t_{1/2} = 5.4 \pm 1.1$ min, $n = 3$) ($p < 0.05$, Student's t test). Figure 7C shows a model where $F278^{7.39}$ may inhibit dissociation (acting like a lid) and the consequence of the $F278^{7.39}$A mutation (Figure 7D). Normal potency may still be achieved in the presence of abnormal binding affinity as the occupancy time is still sufficient for wild-type-like activation despite the more rapid dissociation. An additional mutation ($F278^{7.39}$W) was made in an attempt to try to increase affinity (possibly prolonging the ligand occupancy time within the binding pocket), and perhaps enhance cAMP production. However, such a mutation had no effect on binding or activation ($F278^{7.39}$W $EC_{50} = 2.2 \pm 0.5$ nM, $n = 6$) (Table 1). Although the sum of these data is consistent with our theory, further analysis is needed to confirm these results. However, such assays would require the use of labeled and unlabeled ligands with higher affinities and specific activities (currently not available).

DISCUSSION

The hIP serves important roles in promoting vascular smooth muscle relaxation and inhibiting platelet activation. Previously, we performed site-directed alanine-scanning mutagenesis on a large number of transmembrane amino acids to define the agonist-binding pocket for the hIP (*4*). The central goal of the present study was to elucidate the critical binding-pocket (and neighboring) residues required for transducing the actions of agonist binding to receptor activation. Defects in coupling these two processes are reflected by a change in potency, where higher agonist concentrations (EC_{50}) are required to activate the receptor to the same degree. General transmembrane helical movements required for receptor activation have been determined for a number of G-protein-coupled receptors using elegant techniques such as EPR (*5*, *24*, *25*), the substituted-cysteine-accessibility method (SCAM) (*8*, *26*−*28*), and zinc chelation (*6*, *7*). More specifically, movements in TMIII and TMVI have been shown to be essential for proper activation of many GPCRs including rhodopsin and β_2-AR and parathyroid hormone receptors (*5*−*7*), although the exact molecular mechanism and residues involved have yet to be determined. The majority of these studies, particularly those utilizing EPR and zinc chelation, have focused predominantly on end movements in and around the cytoplasmic face of the receptor. In contrast, our current study is centered upon the potential hIP amino acid requirements at the level of the ligand-binding pocket and surrounding transmembrane domain. Although proper mechanistic evidence is still required to confirm precise α-helical movements, the activation-affecting residues highlighted in this study may help map the potential molecular pathway by which agonist-induced conformational changes drive the signal stimulus through the receptor protein to intracellular effector molecules (presumably via helical movements) to elicit receptor activation. However, it should be noted that mutation-induced protein misfolding may be playing a potential role in functional receptor defects and/or decreased expression. Nevertheless, previous Western analysis on these mutants that were expressed poorly (i.e., D60A, Y75A, F150A, Y188A, D274A F278A, and R279A) (*4*) demonstrated wild-type-like glycosylation patterns, suggesting that severe misfolding was not present. Despite the limitations of overexpression studies, the union of this work, in conjunction with our molecular modeling of the hIP, provides critical information on the specific role of transmembrane residues in binding agonist and eliciting receptor activation.

Structural Analysis Leading to the Cluster Hypothesis (Figure 8). The mechanism by which agonist binding initiates conformational changes within the hIP leading to receptor activation is not known. Upon computer-assisted structural analysis of the residues affecting activation, either exclusively or upon agonist binding, four distinct (spatial) activation clusters of amino acids within the transmembrane domain emerged (Figure 8). The residues comprising each of these clusters play critical roles in the processes of signal transduction and receptor activation, including signal initiation (ligand binding). Moreover, two of the four amino acid clusters were found to contain critical proline residues previously identified to be necessary for hIP activation (P17$^{1.36}$ and P289$^{7.50}$) (*12*). Previous work suggests that proline residues may play an important role, serving as molecular hinges or swivels, aiding in the transmission and amplification of such conformational changes (i.e., α-helical movements) (*12*, *26*). Our study supports this hypothesis asserting that specific ligand−receptor points of contact (occurring upon agonist binding) initiate conformational changes, which transmit (transduce) the signal through adjacent proline and other transmembrane residues. However, specific α-helical movements have yet to be determined for the hIP.

Role of the TMIV/V Cluster (F146$^{4.52}$, F150$^{4.56}$, F184$^{5.40}$, and Y188$^{5.44}$) (Figures 6 and 8). Large, highly conserved hydrophobic residues have been shown to play a critical role in both binding and activation within the regions of TMIV, TMV, and TMVI, across a number of GPCRs (e.g., α_1- and β_2-adrenergic and 5-HT$_2$ receptors) (*8*, *10*, *27*−*29*). Within the hIP receptor, we propose that a number of these large, apolar residues are involved in intra- and inter-α-helical hydrophobic (ring−ring) interactions, which serve as stabilizing forces, allowing the receptor to achieve the active conformation. Extensive EPR studies on the TM α-helical movements of rhodopsin and other GPCRs indicate that TMIV and TMV are relatively immobile in comparison to TMIII and TMVI (*5*−*7*, *30*). Furthermore, stabilization of TMIV and TMV may be required for receptor dimerization (*31*, *32*). Such immobility most likely arises from strong intra- and inter-α-helical interactions, induced by the stacking of large aromatic groups within and between TM α-helices (unlikely to break upon receptor activation) (Figure 6C). Our own data demonstrate that TMIV and TMV of the hIP receptor contain a number of closely associated (stacked) amino acids (i.e., F146$^{4.52}$, F150$^{4.56}$, F184$^{5.40}$, and Y188$^{5.44}$), and are not within the vicinity of the agonist-binding pocket (*4*) (Figure 8). Although the precise role of this cluster remains unclear, its location within TMIV and TMV, and detrimental effect on receptor activation upon mutation, supports its role in intramolecular stabilization.

Further Insights into the hIP Affinity/Potency Relationship. Upon comparing our previously published ligand-binding affinity results (*4*) with our current potency (receptor activation) data (Table 1), four very distinct mutation groups emerged: (1) mutations that exclusively affected potency, (2) mutations that exclusively affected affinity, (3) mutations that perturbed both, and (4) mutations that had no effect on binding or activation. These groups reflect the distinct structural requirements necessary for ligand binding, for receptor activation, and for coupling the two processes. Mutations such as S20$^{1.39}$A, F24$^{1.43}$A, F72$^{2.62}$A, S106$^{3.39}$A, and F184$^{5.40}$A all significantly decrease potency while maintaining normal wild-type binding affinity. There was no significant defect in receptor basal activity (at equivalent expression levels), with activation deficiencies appearing only upon addition of agonist. This suggests that the activation defect arises from a lack of transmission of ligand binding into helical movements necessary for activating Gs, rather than basal uncoupling. Although this is a likely mechanism, as all these residues are in the region of the ligand-binding pocket, definitive determination would require protein purification and the use of such techniques as NMR or EPR. These are currently not feasible with the hIP.

It remains more difficult to assess probable mechanistic roles in activation for those residues that have profound effects on ligand-binding affinity. For binding-pocket mutations R279$^{7.40}$A and Y75$^{2.65}$A, the role in activation seems evident—disruption of the initiating stimulus (i.e., ligand binding), leading to deficient receptor activation. However, in the presence of mutations, the relationship between binding and activation is complex. The contribution of defective binding to activation defects (affinity/potency relationship) is difficult to assess. Further detailed structural analysis is required to parse out this relationship.

Intriguingly, a number of mutations, F278$^{7.39}$A, S68$^{2.58}$A, F97$^{3.30}$A, S185$^{5.41}$A, and D274$^{7.35}$A (Table 1), exhibited a somewhat paradoxical effect, producing significant binding deficits while at the same time sustaining wild-type potency, as measured by cAMP levels. It should be noted that there was no observable increase in basal activity for these mutations to suggest unusually high activation ability in the presence of decreased binding affinity. With mutation F278$^{7.39}$A, we hypothesized that the decreased affinity with wild-type-like potency arose from an increased ligand dissociation rate. In such a situation, iloprost is able to bind and activate the receptor normally (determined by agonist association dynamics and overall receptor occupancy), yet is released very quickly from the binding pocket (i.e., its dissociation rate is drastically increased) due to the site-directed mutation. Thus, the perceived decrease in binding affinity is due to an accelerated off-rate, rather than a deteriorated on-rate (Figure 7). Upon investigation, this notion seems to hold true (for F278$^{7.39}$A), and is supported by an observable increase in ligand dissociation time accounting for the binding defect (Figure 7B). Up to now, the exact role of F278$^{7.39}$ within the ligand-binding pocket was thought to be secondary to that of the important R279$^{7.40}$ residue, which has been shown to form an ionic interaction with the C1-carboxylate group of various hIP ligands. However, these most recent data suggest that F278$^{7.39}$ may serve an equally significant role in retaining agonists within the ligand-binding pocket by acting as a large hydrophobic clamp or lid (Figure 7C,D), interacting with the central rings and α-tail of prostacyclin and its analogues—a concept consistent with our hIP homology model and further verified by a secondary mutation, F278$^{7.39}$W, which exhibited both wild-type-like binding and activation ($K_i = 9.46 \pm 1.2$ nM, $n = 4$, and $EC_{50} = 2.2 \pm 0.5$ nM, $n = 6$). Thus, the presence of a large hydrophobic ring structure (e.g., phenylalanine or tryptophan) at position 278 helps to maintain a prolonged ligand occupancy time. The removal of this residue (F278$^{7.39}$A) produces an apparent defect in binding affinity (due to an accelerated off-rate), but occupancy still remains sufficient

for normal receptor potency. This reproducible phenomenon remains unclear and will require further extensive analysis.

Model of Transmembrane Induction of Activation by Ligand Binding. The culmination of these results provides insight into the specific amino acids involved in hIP receptor activation, delineating the potential molecular pathway by which the ligand-induced signal is transmitted through the transmembrane domain, potentially eliciting conformational changes. We propose that prostacyclin binding initiates α-helical movements at TMII ($Y75^{2.65}$), TMIII ($F95^{3.28}$), and TMVII ($R279^{7.40}$). Furthermore, our results suggest that TMII movement may also induce conformational changes in TMI through an $F72^{2.62}$−$P17^{1.36}$ interaction, in addition to movements in TMVII via $D60^{2.50}$, $D288^{7.49}$, and $P289^{7.50}$. Studies of other GPCRs, such as the GnRH (*33*), ATI receptor (*34*), and 5-HT receptors (*35*), have also suggested that interactions between such specific and highly conserved amino acids localized within TMII and TMVII ($D60^{2.50}$, $D288^{7.49}$, and $P289^{7.50}$) may also contribute to conformational changes and G-protein-mediated signaling. This highly conserved TMVII region has also been shown to be critical for binding and activation of other GPCRs (*36*−*39*). Moreover, proximity to transmembrane prolines (e.g., $P17^{1.36}$ in TMI and $P289^{7.50}$ in TMVII) further suggests that these residues (and associated clusters) may also play major roles in facilitating conformational changes. Additionally, critical hydrophobic ring−ring interactions between TMIV and TMV are necessary for receptor stabilization and normal activation. In agreement with similar investigations of other GPCRs, our data implicate points of activation (conformational changes) involving the proximal binding-pocket region of TMI, TMII, TMIII, and TMVII in coupling agonist binding to hIP receptor activation. At present, further structural analysis regarding the precise movements required for hIP activation is being hampered by the lack of true high-affinity, selective ligands and poor receptor expression. Nevertheless, site-directed mutagenesis, along with molecular homology modeling, provides a powerful means by which to analyze structure−function relationships in the human prostacyclin receptor.

Our major observations in studying the potency effects of ligand-binding-pocket and transmembrane mutations in the human prostacyclin receptor include the identification of four distinct activation clusters that appear to demarcate major areas required for hIP activation (binding pocket, para binding pocket, lower TM movement, and distal TM stabilization). Moreover, these regions have been shown to be composed of both highly conserved ($P289^{7.50}$-associated $D60^{2.50}$ cluster) and unique ($F146^{4.52}$, $F150^{4.56}$, $F184^{5.40}$, and $Y188^{5.44}$) clusters of residues, shown to play important roles in activation of the hIP as well as other GPCRs in general. Such studies will assist in the understanding of conformational changes within the region of the ligand-binding pocket required for coupling the process of agonist binding to activation in many GPCRs.

ACKNOWLEDGMENT

We thank Dr. Kathleen Martin (Departments of Surgery and of Pharmacology & Toxicology, Dartmouth Medical School) for her critiques during the conduction of these studies.

REFERENCES

1. Cheng, Y., et al. (2002) Role of Prostacyclin in the Cardiovascular Response to Thromboxane A2, *Science 296*, 539−541.
2. Billington, C. K., Penn, R. B. (2003) Signaling and regulation of G protein-coupled receptors in airway smooth muscle, *Respir. Res. 4*, 2−23.
3. Miggin, S. M., and Kinsella, B. T. (2002) Investigation of the Mechanisms of G Protein: Effector Coupling by the Human and Mouse Prostacyclin Receptors. Identification of Critical Species-Dependent Differences, *J. Biol. Chem. 277*, 27053−64.
4. Stitham, J., et al. (2003) The Unique Ligand-binding Pocket for the Human Prostacyclin Receptor. Site-Directed Mutagenesis and Molecular Modeling, *J. Biol. Chem. 278*, 4250−7.
5. Farrens, D. L., et al. (1996) Requirement of rigid-body motion of transmembrane helices for light activation of rhodopsin, *Science 274*, 768−70.
6. Sheikh, S. P., et al. (1996) Rhodopsin activation blocked by metal-ion-binding sites linking transmembrane helices C and F, *Nature 383*, 347−50.
7. Sheikh, S. P., et al. (1999) Similar structures and shared switch mechanisms of the beta2-adrenoceptor and the parathyroid hormone receptor. Zn(II) bridges between helices III and VI block activation, *J. Biol. Chem. 274*, 17033−41.
8. Chen, S., et al. (2002) Phe(303) in TMVI of the alpha(1B)-adrenergic receptor is a key residue coupling TM helical movements to G-protein activation, *Biochemistry 41*, 588−96.
9. Chen, S., et al. (2002) Mutation of a single TMVI residue, Phe(282), in the beta(2)-adrenergic receptor results in structurally distinct activated receptor conformations, *Biochemistry 41*, 6045−53.
10. Chen, S., et al. (1999) Phe310 in Transmembrane VI of the alpha 1B-Adrenergic Receptor Is a Key Switch Residue Involved in Activation and Catecholamine Ring Aromatic Bonding, *J. Biol. Chem. 274*, 16320−16330.
11. Roth, B. L., et al. (1998) 5-Hydroxytryptamine2-family receptors (5-hydroxytryptamine2A, 5-hydroxytryptamine2B, 5-hydroxytryptamine2C): where structure meets function, *Pharmacol. Ther. 79*, 231−57.
12. Stitham, J., Martin, K. A., and Hwa, J. (2002) The critical role of transmembrane prolines in human prostacyclin receptor activation, *Mol. Pharmacol. 61* (5), 1202−10.
13. Stitham, J., Stojanovic, A., and Hwa, J. (2002) Impaired receptor binding and activation associated with a human prostacyclin receptor polymorphism, *J. Biol. Chem. 277*, 15439−44.
14. Teller, D. C., et al. (2002) Advances in determination of a high-resolution three-dimensional structure of rhodopsin, a model of G-protein-coupled receptors (GPCRs), *Biochemistry 40*, 7761−72.
15. Guex, N., and Peitsch, M. C. (1997) SWISS-MODEL and the Swiss-PdbViewer: an environment for comparative protein modeling, *Electrophoresis 18*, 2714−23.
16. Ballesteros, J. A., Weinstein, H. (1995) Integrated Methods for the Construction of Three-Dimensional Models and Computational Probing of Structure−Function Relations in G Protein-Coupled Receptors, in *Receptor Molecular Biology* (Sealfon, S., Ed.) pp 366−428, Academic Press, New York.
17. Hwa, J., et al. (1997) Synergism of constitutive activity in alpha 1-adrenergic receptor activation, *Biochemistry 36*, 633−9.
18. Liu, I. S., et al. (1996) Dopamine D4 receptor variant in Africans, D4valine194glycine, is insensitive to dopamine and clozapine: report of a homozygous individual, *Am. J. Med. Genet. 61*, 277−82.
19. Miura, S., Zhang, J., and Karnik, S. S. (2000) Angiotensin II type 1 receptor-function affected by mutations in cytoplasmic loop CD, *FEBS Lett. 470*, 331−5.
20. Noda, K., et al. (1994) The high affinity state of the beta 2-adrenergic receptor requires unique interaction between conserved and non-conserved extracellular loop cysteines, *J. Biol. Chem. 269*, 6743−52.
21. Neubig, R. R., et al. (2003) International Union of Pharmacology Committee on Receptor Nomenclature and Drug Classification. XXXVIII. Update on terms and symbols in quantitative pharmacology, *Pharmacol. Rev. 55*, 597−606.
22. Ostrom, R. S., Post, S. R., and Insel, P. A. (2000) Stoichiometry and compartmentation in G protein-coupled receptor signaling:

implications for therapeutic interventions involving G(s), *J. Pharmacol. Exp. Ther. 294*, 407−12.
23. Ostrom, R. S., et al. (2001) Receptor number and caveolar co-localization determine receptor coupling efficiency to adenylyl cyclase, *J. Biol. Chem. 276*, 42063−9.
24. Altenbach, C., et al. (2001) Structure and function in rhodopsin: mapping light-dependent changes in distance between residue 316 in helix 8 and residues in the sequence 60−75, covering the cytoplasmic end of helices TM1 and TM2 and their connection loop CL1, *Biochemistry 40*, 15493−500.
25. Altenbach, C., et al. (2001) Structure and function in rhodopsin: mapping light-dependent changes in distance between residue 65 in helix TM1 and residues in the sequence 306−319 at the cytoplasmic end of helix TM7 and in helix H8, *Biochemistry 40*, 15483−92.
26. Sansom, M. S., and Weinstein, H. (2000) Hinges, swivels and switches: the role of prolines in signalling via transmembrane alpha-helices, *Trends Pharmacol. Sci. 21*, 445−51.
27. Waugh, D. J., et al. (2000) Novel aromatic residues in transmembrane domains IV and V involved in agonist binding at alpha-(1a)-adrenergic receptors, *J. Biol. Chem. 275*, 11698−705.
28. McAllister, S. D., et al. (2002) A critical role for a tyrosine residue in the cannabinoid receptors for ligand recognition, *Biochem. Pharmacol. 63*, 2121−36.
29. Javitch, J. A., et al. (1998) A cluster of aromatic residues in the sixth membrane-spanning segment of the dopamine D2 receptor is accessible in the binding-site crevice, *Biochemistry 37*, 998−1006.
30. Altenbach, C., et al. (1996) Structural features and light-dependent changes in the cytoplasmic interhelical E−F loop region of rhodopsin: a site-directed spin-labeling study, *Biochemistry 35*, 12470−8.
31. Liang, Y., et al. (2003) Organization of the G Protein-coupled Receptors Rhodopsin and Opsin in Native Membranes, *J. Biol. Chem. 278*, 21655−62.
32. Fotiadis, D., et al. (2003) Atomic-force microscopy: Rhodopsin dimers in native disc membranes, *Nature 421*, 127−8.
33. Flanagan, C. A., et al. (1999) The functional microdomain in transmembrane helices 2 and 7 regulates expression, activation, and coupling pathways of the gonadotropin-releasing hormone receptor, *J. Biol. Chem. 274*, 28880−6.
34. Miura, S., et al. (2003) TM2-TM7 interaction in coupling movement of transmembrane helices to activation of the angiotensin II type-1 receptor, *J. Biol. Chem. 278*, 3720−5.
35. Sealfon, S. C., et al. (1995) Related contribution of specific helix 2 and 7 residues to conformational activation of the serotonin 5-HT2A receptor, *J. Biol. Chem. 270*, 16683−8.
36. Wess, J., et al. (1993) Functional role of proline and tryptophan residues highly conserved among G protein-coupled receptors studied by mutational analysis of the m3 muscarinic receptor, *EMBO J. 12*, 331−8.
37. Kolakowski, L. F., et al. (1995) Probing the "message:address" sites for chemoattractant binding to the C5a receptor. Mutagenesis of hydrophilic and proline residues within the transmembrane segments, *J. Biol. Chem. 270*, 18077−82.
38. Fernandez, L. M., and Puett, D. (1996) Identification of amino acid residues in transmembrane helices VI and VII of the lutropin/choriogonadotropin receptor involved in signaling, *Biochemistry 35*, 3986−93.
39. Hong, S., et al. (1997) Roles of transmembrane prolines and proline-induced kinks of the lutropin/choriogonadotropin receptor, *J. Biol. Chem. 272*, 4166−71.

BI0496788